IEEE Access
Multidisciplinary | Rapid Review | Open Access Journal

Received April 9, 2020, accepted April 20, 2020, date of publication April 23, 2020, date of current version May 15, 2020.

Digital Object Identifier 10.1109/ACCESS.2020.2989756

Dual-Function Enhancer for Near-Infrared Photopolymerization: Kinetic Modeling for Improved Efficacy by Suppressed Oxygen Inhibition

YIN-CHEN CHIU[1], DA-CHUAN CHENG[2], JUI-TENG LIN[3], KUO-TI CHEN[4], AND HSIA-WEI LIU[5]

[1]Graduate Institute of Applied Science and Engineering, Fu Jen Catholic University, New Taipei City 242, Taiwan
[2]Department of Biomedical Imaging and Radiological Science, China Medical University, Taichung 404, Taiwan
[3]Photon Vision, Inc. Taipei City 242, Taiwan
[4]Graduate Institute of Applied Science and Engineering, Fu Jen Catholic University, New Taipei City 242, Taiwan
[5]Department Life Science, Fu Jen Catholic University, New Taipei City 242, Taiwan

Corresponding author: Hsia-Wei Liu (079336@gmail.com)

Author HW Liu thanks the financial support from Ministry of Science and Technology (MOST) under Grant number 107-2622-E-030-001-CC3. Author DC Cheng thanks the financial support from China Medical University under Grant number CMU 108-S-25.

ABSTRACT There are many strategies for improved conversion efficacy such as the reduction of oxygen inhibition effects (OIH). Three-component system using the phosphine to reduce the OIH effects during the free radical polymerization of (meth)acrylate monomers has been reported. Addition, near-infrared (NIR) photopolymerization offers advantages of safer, less light diffusion and scattering, and deeper penetration into the materials. This study presents the detailed kinetics, and modeling the conversion efficacy associated with the experimental results of Bonardi *et al.* (Macromolecules, 2018, 51, 1314-1324). The dual function of the enhancer additive includes: (i) regenerating the photoinitiator, and (ii) producing extra reactive radical. The temporal profiles of the concentration of each of the 3-component system and the associate conversion efficacy are numerically produced. In this study, several new findings showing unique features of various factors influencing the conversion will be demonstrated. For examples, reverse trends (roles) are found in: (i) the light intensity and enhancer concentration, and (ii) the coupling rate constants of radical-oxygen and radical-monomer. The monomer conversion is an increasing function of enhancer, oxygen concentration, and the light intensity. However, they have significantly different steady state features. The steady-state conversion increases from 10% without the enhancer (with enhancer concentration $[B]_0 = 0$) to (30%, 50%, 80%) for $[B]_0 = (0.5, 1.0, 2.0)\%$. High conversion also requires a long lifetime of the free radical. Finally, the measured conversion profiles at various conditions reported by Bonardi *et al.* (Macromolecules, 2018, 51, 1314-1324) are compared and analyzed by our modeling.

INDEX TERMS Kinetic model, photopolymerization, conversion efficacy, oxygen inhibition, near IR.

I. INTRODUCTION

Free radical photopolymerization consists of two types of photoinitiation (PI), in which type-I is related to the direct coupling of the UV-light initiated radical and the monomers; whereas type-II is related to oxygen-mediated crosslink, or visible-light initiated radicals which coupled to the co-initiator [1], [2]. UV lights (360-400 nm) have been commonly used in most type-I photopolymerization of (meth)acrylate monomers [1]–[3]. However, the UV wavelength suffers the disadvantages of being unsafe to skin and eyes, small penetration depth and larger light scattering in tissues [1]. Camphorquinone (CQ), due to its good visible absorption properties, is the most common type-II PI of (meth)acrylates under visible light [4]–[8]. The first three-component system of (CQ)/amine/ (aryliodonium ylides) was reported by Kirschner *et al.* [8].

In comparison, near-infrared (NIR) light offers advantages of safer, less light diffusion and scattering, and deeper penetration into the materials [1], [2]. Thus, the curing of a thick and filled material can be potentially enhanced compared to curing with UV or visible light. However, the use of NIR

The associate editor coordinating the review of this manuscript and approving it for publication was Navanietha Krishnaraj Krishnaraj Rathinam.

photoinitiation systems such as cyanine is often associated with a low reactivity and requires a high light intensity [1]. Phthalocyanines and conjugated macrocycles have been used as commercial pigments and dyes having a high molar absorptivity coefficient in the red and NIR wavelength of 650-810 nm [9], [10]. Efficient polymerization conversions using NIR photoinitiation by cyanine/iodonium salt couples are reported by Strehmel *et al* [9]. Three-component system with a dye as a photosensitizer absorbing in the NIR range, an iodonium salt (as an initiator), and a phosphine (as a co-initiator) was reported, in which the phosphine is used to reduce oxygen inhibition (OIH) during the free radical polymerization of (meth)acrylate monomers [10], [11].

There are many other strategies to reduce (OIH) including: working in an inert or closed environment, increasing the photoinitiator concentration, increasing the light dose, or light intensity, use of multiple photoinitiators with different rate of initiation, or addition of oxygen scavengers [12], [13]. Furthermore, functionalized monomers which are insensitive to oxygen, such as the thiol-ene and thiol-acrylate-Michael additive systems were also reported [14], [15]. Additive enhancer-monomer were also proposed to improve the curing (crosslink) efficacy by either reducing the oxygen inhibition effect by stable-monomer, or increase the lifetime of radicals in clinical applications [16], [17]. In addition, dual-wavelength (red and UV) photopolymerization was reported, in which pre-irradiation of red-light was used to pre-reduce the OIH [18].

Recently, Bonardi *et al* [19] reported the first three-component system for high performance NIR (785 nm) photopolymerization of thick methacrylates, which used (i) a borate dye used as a NIR photosensitizer (PS), (ii) an iodonium salt as a photoinitiator (PI) for the free radical polymerization of the (meth)acrylates, and (iii) a dual-function enhancer (phosphine) to prevent oxygen inhibition, and to regenerate the PS upon irradiation, in which a stable radical is coupled with the enhancer.

This study presents the detailed kinetics, and modeling the conversion efficacy associated with the experimental results of Bonardi *et al* [19]. The dual function of the enhancer additive includes (i) prevention of OIH, and (ii) regeneration of the PS, which will be explored numerically and analytically in a 3-initiator system. The temporal profiles of the concentration of each of the 3-component and the associate conversion efficacy are numerically produced. In this study, several new findings showing unique features of various factors influencing the conversion will be demonstrated. For examples, the reverse trends (roles) are found in: (i) the light intensity and enhancer concentration on the PS concentration; and (ii) the coupling rate constants of radical-oxygen and radical-monomer coupling. Finally, the measured conversion profiles at various conditions reported by Bonardi *et al* [19] are compared and analyzed by our modeling.

We note that due to the complexity of the kinetics, this article is highly theoretical. Therefore, for those readers without a strong theoretical background may skip the mathematical portion and focus on the kinetics shown by Fig. 1 and section *3.3. Summary of important features* which provides all the important issues explored by this article. In addition, readers may read the measured data reported by Bonardi *et al* [19] which also explained the important features as predicted by our analytic formulas.

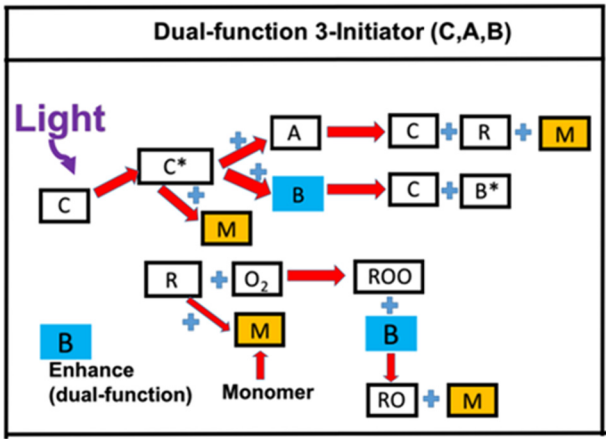

FIGURE 1. Schematics of photochemical mechanisms in a 3-initiator (C/B/A) system under an NIR exposure; in which the initiator dye (C) is excited to its excited state C* which could react with [A] to regenerate [C], and produce active radical (R). R could initiate crosslink of the monomer [M] or react with oxygen producing a radical [ROO], which reacts with [B] to produce radical [RO] causing extra crosslink of [M].

II. MATERIALS AND METHODS

A. PHOTOCHEMICAL KINETIC

As shown by Fig. 1, the kinetic scheme of a 3-initiator system, [C], [A] and [B], in the presence of oxygen is proposed. Under the NIR exposure, the initiator dye (C) is exited to its excited-state, or triplet-excited state, given by C^*, which could react with initiator [A] to produce active radical (R) or react with co-initiator [B]; where dye [C] is regenerated in both reactions. The coupling of radical [R] and oxygen [O2] produces a peroxyl radical [ROO], which is too stable for the polymerization to proceed. Therefore, an enhancer-initiator [B] is required to create less stable radical [RO] for extra crosslinks of the monomer, [M]. We note that the initiator [B] plays a dual-function of: (i) regeneration of dye [C], and (ii) reducing OIH by generating an extra active radical [RO] for improved conversion. Without the dual-function enhancer [B], OIH reduces the radical [R] and the conversion efficacy, in which an induction time is defined for the delayed rising of the conversion curve [13].

Example of above system was reported by Kirschner *et al* [8], in a 3-component system of C/B/A, in which [C] = IR-140 borate, [B] = 4-(Diphenylphosphino) benzoic acid (4-dppba), and [A] = iodonium salt Ar2I+PF6−, with initial concentration of [0.1/2.0/3.0] wt%, and mixed in a monomer [M] = methacrylate.

The kinetic equations for our previous single-initiator systems are revised for the 3-initiator system as follows [9]–[12]

$$\frac{\partial[C]}{\partial t} = -bI[C] + (k_1[A] + k_2[B] + k_5)\,C^* \qquad (1)$$

$$\frac{\partial[\mathrm{A}]}{\partial \mathrm{t}} = -\mathrm{k}_1 C^*[\mathrm{A}] \quad (2)$$

$$\frac{\partial[\mathrm{B}]}{\partial \mathrm{t}} = -\mathrm{k}_2 C^*[\mathrm{B}] - \mathrm{k}_4[\mathrm{ROO}][\mathrm{B}] \quad (3)$$

$$\frac{\partial \mathrm{C}^*}{\partial \mathrm{t}} = \mathrm{bI}[\mathrm{C}] - (\mathrm{k}_1[\mathrm{A}] + \mathrm{k}_2[\mathrm{B}] + \mathrm{k}_7[\mathrm{M}] + \mathrm{k}_5) C^* \quad (4)$$

$$\frac{\partial[\mathrm{ROO}]}{\partial \mathrm{t}} = \mathrm{k}_3 \mathrm{R}[O_2] - \mathrm{k}_4[\mathrm{ROO}][\mathrm{B}] + \mathrm{k}_6[\mathrm{RO}] \quad (5)$$

$$\frac{\partial[\mathrm{RO}]}{\partial \mathrm{t}} = \mathrm{k}_4[\mathrm{ROO}][\mathrm{B}] - (\mathrm{k}_6 + \mathrm{k}_5[\mathrm{M}])[\mathrm{RO}] \quad (6)$$

$$\frac{\partial[\mathrm{R}]}{\partial \mathrm{t}} = \mathrm{k}_1 C^*[\mathrm{A}] - (\mathrm{k}'[\mathrm{M}] + \mathrm{k}''[\mathrm{O}_2])[\mathrm{R}] - 2\mathrm{k}_\mathrm{T}[R]^2 \quad (7)$$

$$\frac{\partial[\mathrm{O}_2]}{\partial \mathrm{t}} = -\mathrm{k}_3[\mathrm{R}][O_2] \quad (8)$$

$$\frac{\partial[\mathrm{M}]}{\partial t} = -(\mathrm{k}_7 C^* + \mathrm{k}_5[\mathrm{RO}] + \mathrm{k}'[\mathrm{R}])[\mathrm{M}] \quad (9)$$

where b=83.6a'wq, with w being the NIR light wavelength (in cm) and q is the excited state C* quantum yield, a' is the mole absorption constant, in (1/mM/%) and light intensity, I (z, t) in mW/cm2.

We will use the so-called quasi-steady state assumption [5] described as follows. The life time of radical C* and [RO] are very short (ns to μs time scale) since they either decay or react with the substrate monomer after they are created. However, [ROO] is a rather stable radical and could not be assumed at a steady-state. The steady-state solutions of Eq. (4) to (6) for the radicals of C* and [RO] lead to C* = bIg[C], and [RO] = k4g'[ROO][B], with g = k7/(k5+k1[A]+k2[B]+k7[M]), and g'=1/(k6+k'5[M]), kij=(ki/kj). Using these steady-state values, Eq. (1) to (9) reduce to

$$\frac{\partial[\mathrm{C}]}{\partial \mathrm{t}} = -\mathrm{B}_3[\mathrm{M}] \quad (10)$$

$$\frac{\partial[\mathrm{A}]}{\partial \mathrm{t}} = -\mathrm{k}_1 \mathrm{B}_3[A] \quad (11)$$

$$\frac{\partial[\mathrm{B}]}{\partial \mathrm{t}} = -\mathrm{k}_2 \mathrm{B}_3[B] - [\mathrm{RO}]/\mathrm{g}' \quad (12)$$

$$\frac{\partial[\mathrm{ROO}]}{\partial \mathrm{t}} = \mathrm{k}_3[\mathrm{R}][\mathrm{O}_2] - \mathrm{k}_5[M][\mathrm{RO}] \quad (13)$$

$$\frac{\partial[\mathrm{R}]}{\partial \mathrm{t}} = \mathrm{k}_1 \mathrm{B}_3[\mathrm{A}] - (\mathrm{k}'[\mathrm{M}] + \mathrm{k}_3[\mathrm{O}_2])[\mathrm{R}] - 2\mathrm{k}_\mathrm{T}[R]^2 \quad (14)$$

$$\frac{\partial[\mathrm{O}_2]}{\partial \mathrm{t}} = -\mathrm{k}_3[R][O_2] \quad (15)$$

$$\frac{\partial[\mathrm{M}]}{\partial \mathrm{t}} = -(\mathrm{B}_3 + \mathrm{k}_5[\mathrm{RO}] + \mathrm{k}'[\mathrm{R}])[\mathrm{M}] \quad (16)$$

where B3 = gbI[C] and the steady-state radical [RO] = k4g'[ROO][B], or [RO] = (k3/k5)(R[O2]/[M]), if we also use the steady state of [ROO] in Eq. (5). We note that the radical [R] and conversion is a decreasing function of the oxygen initial concentration, as shown by Eq. (14), whereas conversion is improved by enhancer [B] via its dual function of (i) regenerating the dye [C], and (ii) generating extra radical [RO], as shown by the second term of Eq. (16), k5[RO].

The dynamic light intensity is given by [9], [10]

$$\frac{\partial \mathrm{I(z,t)}}{\partial \mathrm{z}} = -\mathrm{A}'(z,t) I(z,t) \quad (17)$$

$$\mathrm{A}'(\mathrm{z,t}) = 2.3[(\mathrm{a}' - \mathrm{b}')[\mathrm{C}](\mathrm{z,t}) + \mathrm{b}'\mathrm{C}_0\mathrm{F}' + \mathrm{Q}'] \quad (18)$$

where a' and b' are the extinction coefficients of Initiator-C and the photolysis product, respectively; Q' is the absorption coefficient of the monomer at NIR wavelength. All the reaction rate constants are defined by the associated coupling terms. For examples, in Eq. (4), k' and k'' are the coupling of [R] and [M], and R and oxygen [O2], respectively; and a bimolecular termination rate of kT; R also couples with initiator [A] and [B] by a rate constant of k1 and k2, respectively. Greater detail may be found in Ref. [9], [10]. We note that the dynamic feature of Eq. (17) due to the depletion of C(z,t) and the spatial dependence of both I(z,t) and C(z,t) are critical in optically-thick polymers [10].

The steady-state radical of Eq. (13) is given by

$$R = \left(\frac{1}{4\mathrm{k}_\mathrm{T}}\right)(-G + \sqrt{G^2 + 8\mathrm{k}_T bIg[C][A]}) \quad (19)$$

where G = k'[M]+k$_3$[O$_2$].

For the radical [R] dominant case with $8\mathrm{k}_\mathrm{T}\mathrm{bIC} \gg \mathrm{G}^2$, we obtain an approximate radical given by

$$R = \sqrt{0.5(bIg[C][A])/\mathrm{k}_T} - G/(4\mathrm{k}_T) \quad (20)$$

which is a decreasing function of the oxygen inhibition term G. We note that the conversion is a decreasing function of the oxygen initial concentration, whereas conversion is improved by enhancer [B] via the dual function of (i) regeneration of dye [C], and (ii) reducing OIH by generating an extra active radical [RO].

B. ANALYTIC FORMULAS FOR EFFICACY

The monomer conversion efficacy for a bimolecular termination process is given by CEFF = 1-[M]/[M]$_0$ = 1-exp(-S), with [M]$_0$ being the initial monomer concentration, and the S-function is given by the time integral of the total rate factor R$_\mathrm{T}$ given by, d[M]/dt= -R$_\mathrm{T}$[M], in which RT has two components given by Eq. (16).

Solutions of Eq. (10) to (18) are available by the approximated analytic formulas for I$_\mathrm{j}$(z,t) as follow [2], [4]

$$I(z,t) = I_0 \exp\left[-A'z\right] \quad (21)$$

$$A'(\mathrm{z,t}) = 2.3(\mathrm{a}'C_0 + \mathrm{Q}) - A_1\mathrm{t} \quad (22)$$

where A$_1$ = 2.3(a'-b')C0I0bz. We note that the –A$_1$t term represents the decrease of A', or increase of light intensity due to PS depletion, which is important for optically-thick polymers.

Using Eq. (21) and for (k$_{57}$ +k$_{17}$[A]+k$_{27}$[B])$\ll$[M], g=1/[M], solution of Eq. (10) gives us

$$C(z,t) = C_0 \exp\left[-B'(t)\right] \quad (23)$$

$$B'(t) = b\int I(z,t)\,[1 - H(t)]dt \quad (24)$$

where H(t)=(k$_{57}$+k$_{17}$[A]+k$_{27}$[B])/[M]. We note that C(z,t) has a longer lifetime or reduced decaying rate due to the H-factor proportional to k$_{17}$[A]+k$_{27}$[B]), which could enhance the efficacy. As shown by Eq. (18), larger C(z,t) enhanced by H-factor will improve the efficacy by an increased radical R.

When H=0, analytic solutions of C(z,t) and efficacy are available as follows

$$C(z,t) = C_0 \exp\left[-B't\right] \tag{25}$$

where B'= $bI_0\exp(-A''z)-0.5A_1t$, with $A_0 = 0.5 \times 2.3(a'+b') + 2.3Q$, A'' being the averaged absorption given by A''= $0.5 \times 2.3(a'+b')+2.3Q$. Given above C, we may find the radical of Eq. (20) and then the conversion efficacy C_{EEF} = 1-exp(-S), with S(z,t) given by, for g'≪k', and ignored A1,

$$S = KG(z,t)\sqrt{0.5bXI_0C_0} \tag{26}$$

$$G'(z,t) = [1-\exp[-B''t)]/B'' \tag{27}$$

where K=k'/$k_T^{0.5}$, B''=0.5(B'-$0.5A_1$t), X=exp[-A_2z]. We note that when H-factor is included, B'' is reduced with higher S and conversion.

For analytic solution of Eq. (23), we could solve for the approximated solution of Eq. (11) and (12) for [A] and [B] as follows: $[A]=[A]_0-bIC_0G'$, and $[B]=[B]_0-bIC_0G'$. Therefore, the time integral of H(t) proportional to $([A]_0+[B]_0)t$ less than the time integral of G'(t). Eq. (25) shows B'(t) is reduced by a factor proportional to $([A]_0+[B]_0)$ t, which enhanced the conversion, comparing to when [A]+[B]=0. Numerical solutions of Eq. (15) will be shown later, without the above described assumptions.

For the case when k_5[RO] is dominant in Eq. (16), given the steady-state solution of Eq. (5) and (6) leads to [RO]= $(k_3/k_5)(R[O_2]/[M])$, which gives the solution of Eq. (16)

$$M(t) = M_0 - k_3\int_0^t [R][O_2]dt \tag{28}$$

Therefore, by the definition of efficacy C_{EFF} = 1-M/M_0, we obtain

$$C_{EFF} = \left(\frac{k_3}{M_0}\right)\int_0^t [R][O_2]dt \tag{29}$$

where radical [R] is proportional to bICg, but is a decreasing function of oxygen, as shown by Eq. (20). We note that g= $k_7/(k_5 + k_1[A]+ k_2[B]+ k_7[M])$, and g'=$1/(k_6+ k_5'[M])$, are decreasing function of the rate constant k_5 and k_5', and inverse proportional to the life time of C* and [RO], respectively. We note that there is no analytic solution for Eq. (29), which could be solved only numerically [R] and $[O_2]$ to obtain the time integral. Numerical results will be shown later.

III. RESULTS AND DISCUSSION

If We note that the radical [R] and conversion is a decreasing function of the oxygen initial concentration, as shown by Eq. (14), whereas conversion is improved by enhancer [B] due to its dual function of: (i) regenerate the dye [A], and (ii) generate extra radical [RO], as shown by the second term of Eq. (16), k_5[RO]. The influencing factors of conversion to be explored numerically include: the initial concentrations $[A]_0$, $[B]_0$, C_0 and oxygen $[O_2]_0$, the coupling constant B_3 = gbIC, the g-functions g and g', and the rate constants, k_{ij}, specially k_5, the coupling between [RO] and [M]. We note the coupling constant bI, a product of b and light intensity (I), will be considered as one parameter which also represents the light intensity for a given absorption constant (b).

A. DYNAMIC PROFILES

Figure 2 shows the role of the enhancer initial concentration $[B]_0$ (shown by Figure (A), and the coupling constant bI_0 (shown by Figure (B), for fixed $[A]_0$, $[C]_0$ and $[O_2]_0$. These profiles show that the conversion is an increasing function of $[B]_0$ and bI_0. However, unlike Figure (A), Figure (B) shows the same steady-state conversion. This feature could be realized by the radical [RO] profiles shown in Figure 3, in which Figure 3(A) shows increasing areas covered by curves 1,2,3, and 4. In contrast, Figure 3(B) shows the same the area covered by all 4 curves. Our new finding could be further explored by Eq. (16) that when the second term, k_5[RO], is dominant, the efficacy is mainly governed by the time integral or the area covered by the [RO] profile shown in Figure 3. This also demonstrates the consistent trends of Figure (A) and (B) in Figure 2 and Figure 3.

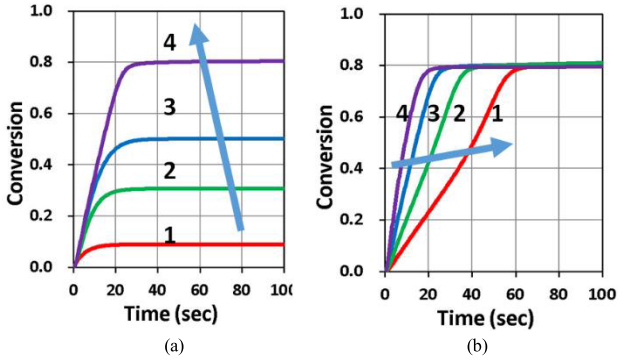

FIGURE 2. Conversion profiles for: (a) concentration $[B]_0$ = (0,0.5,1.0, 2.0) %, for curve (1,2,3,4); with $[A]_0$ = 3.0%, $[C]_0$ = 0.1%, b'= bI_0 = 0.6 (1/s/%); and (b) coupling constant b'= bI_0 = (0.15,0.3,0.6,1.2) (1/s/%), with $[A]_0$ = 3.0%, $[B]_0$ = 2.0%, $[C]_0$ = 0.1%, $[O_2]_0$ = 1.5mg/L; and k'=0.7, k''=2.5, $k_T = k_2 = 2.0$, $k_1 = 0.7$, $k_3 = 8$, $k_5 = k_7 = 1$ (1/s).

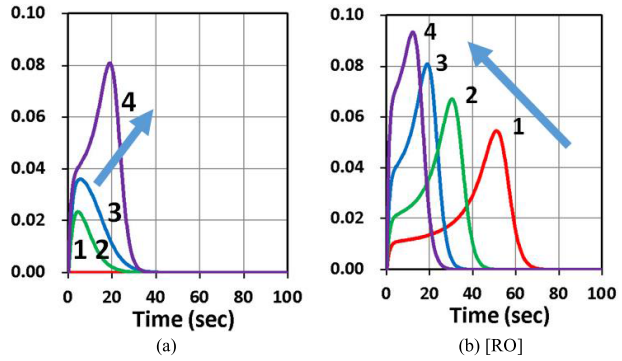

FIGURE 3. The radical [RO] profiles associate to Figure 2 for various $[B]_0$, shown by (a); and for various bI_0, shown by (b).

The peaks of [RO] profiles shown in Figure 3 could be further interpreted as follows. As shown by Figure 1 and Eq. (5) and (6), generation of [RO] is governed by the radical [R]

and oxygen $[O_2]$, in which [R] and $[O_2]$ are, respectively, an increasing and decreasing function of time. Therefore, the combined effect leads to the optimal (or peak) of the temporal profile of [RO]. Furthermore, a larger co-initiator concentration ($[B]_0$ leads to a larger radical [RO] as shown in Figure 3 (A). In contrast, a higher light intensity leads to a faster oxygen depletion and thus a faster drop of [RO] profile as shown in Figure 3 (B).

Figure 4 and 5 show the concentration profiles of initiator C(t), and oxygen $[O_2]$ associate to Figure 2(A) and 2(B), respectively. We note that C(t) has a higher value in the presence of enhancer ([B]) due to the regeneration of C, shown by Figure 4 having various $[B]_0$. In contrast, a reversed trend is shown by Figure 5 having various coupling constant of b'= bI0, in which a larger b' leads to a stronger depletion and lower value of C(t).

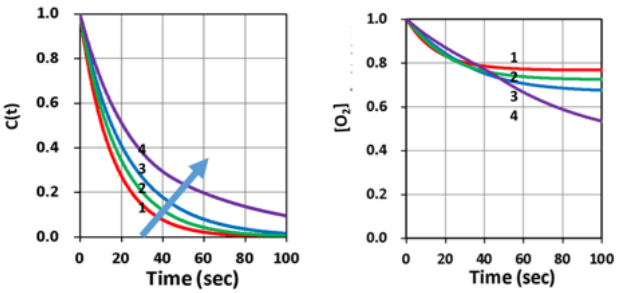

(a) C(t) (b) $[O_2](t)$

FIGURE 4. The concentration profiles of initiator C(t), and oxygen $[O_2]$ associate to Figure 2(a).

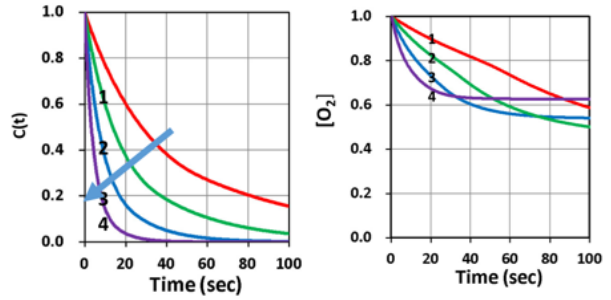

(a) C(t) (b) $[O_2](t)$

FIGURE 5. Same as Figure 4, but associate to Figure 2(B).

Figure 6 shows the role of oxygen–that a higher initial oxygen concentration achieves a higher efficacy, as also predicted Eq. (16) which has three components given by $B_3 =$ gbIC, k_5[RO] and k'R. The steady-state solution of Eq. (5) and (6) leads to $k_5[RO]=k_3(R[O_2]/[M])$, which is an increasing function of oxygen. In the absence of oxygen, radical [RO]=0, the efficacy is given by gbIC and k'R, as shown by curve-1 of Figure 6(B). In contrast, for the k'R dominant case, conversion is reduced by OIH, as shown by Eq. (20), in which bimolecular termination leads to a reverse-trend of light intensity, i.e., a lower intensity leads to a higher steady state conversion.

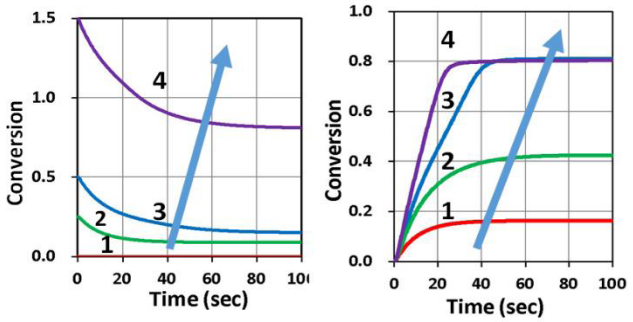

(a) (b)

FIGURE 6. The oxygen profile (a), and conversion profile (b), for various initial oxygen concentration of $[O_2]_0$ = (0,0.25,0.5,1.5) mg/L, with $[A]_0$ = 3.0%, $[B]_0$ = 2.0%, $[C]_0$ = 0.1%, bI_0 = 0.6 (1/s/5).

Figure 7(A) shows that efficacy is an increasing function of k_3, (a reaction rate between [R] and $[O_2]$), but a decreasing function of the rate constant k_5. This reverse-trend could be realized by $B_3 =$ gbI[C], which is a decreasing function of the rate constant k_5. We note that g= $k_7/(k_5 + k_1[A]+ k_2[B]+ k_7[M])$, and g'=$1/(k_6+ k_5'$ [M]), are decreasing function of the rate constant k_5 and k_5', which are inverse proportional to the life time of C* and [RO], respectively. Therefore, shorter radical life time (or larger k_5) of C* or [RO] leads to lower conversion. To achieve a higher conversion a longer lifetime (or smaller k_5) is requires.

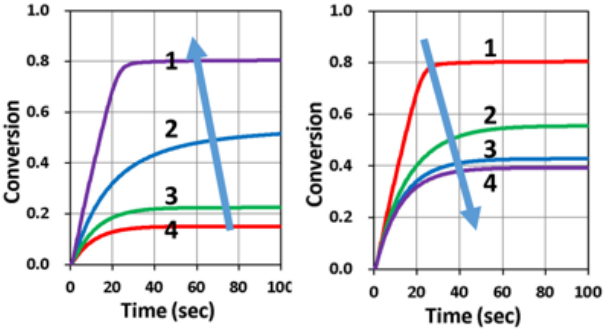

(a) k_3 (b) k_5

FIGURE 7. Conversion profiles for various rate constants: (a) k_3 = (1,2,4,8) (1/s); and (b) k_5 = (1,2,4,8) (1/s), with other fixed parameters same as that of Figure 2.

B. ANALYSIS OF MEASURED DATA

The measured data shown by Figures 4, 6 and 10 of Bonardi *et al* [19] could be compared to our modeled results as follows. Figure 8 shows that higher coupling constant b'= bI0 leads to higher efficacy, which is also an increasing function of light intensity, as shown by Figures 4, 6 and 8 of Bonardi *et al* [19]. Furthermore, the photolysis (% decomposition of the peak at 800 nm) upon laser diode at 785 nm, shown by Figure 10 of Bonardi *et al* [19] could be compared with our Figure 4(A) for the initiator concentration C(t), in which a higher enhancer concentration [B] leads to a higher C(t), or less depletion due to the regeneration of C(t) by the enhancer [B]. We note that the photolysis or the

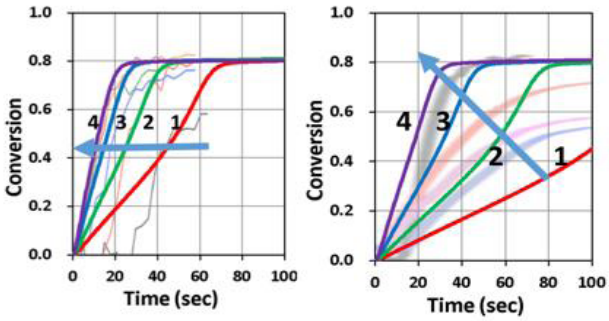

FIGURE 8. Calculated conversion profiles for various coupling constant b′= bI_0: (A) b′= (0.12,2.4,4.8,7.6) (1/s/%), and (B) b′= (0.05,0.1,2.0,4.0) (1/s/%), for curves (1,2,3,4); where b′ is fit to the measured profiles under NIR 785 nm diode laser with light intensity of I_0=(0.4,2.08,2.34,2.55) (mW/cm^2), shown by background curves (replot from Figure 4 and 6 of Bonardi *et al* [19]).

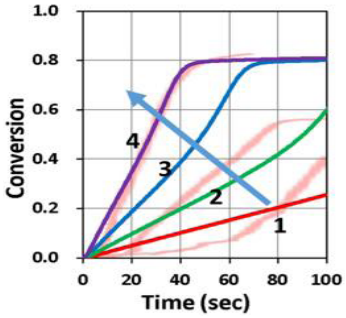

FIGURE 9. Same as Figure 8, but for fit coupling constant b′= bI_0 = (0.03, 0.06,0.12,0.24) (1/s/%), background curves (replot from Figure 10 of Bonardi *et al* [19]).

relative peak spectrum height at 800 nm, D(t) reported by Bonardi *et al* [19], is related to C(t) by D(t) =C(t)/C_0.

Numerical results shown by Figs. 2 to 10, and our analytic formulas provide the following important features:

(i) The radical [R] and conversion are reduced by the oxygen inhibition, as shown by Eq. (14), whereas conversion is improved by enhancer [B] via dual function of (i) regenerate the dye [C], and (ii) generate extra radical [RO], as shown by the second term of Eq. (16), k_5[RO].

(ii) The conversion is an increasing function of enhancer concentration $[B]_0$ and the coupling constant, b′= bI_0, as shown by Figure 2. However, they have significantly different steady state feature, as shown by Figure 2, in which Figure 2(B) shows the same steady-state conversion for different values of b′.

(iii) As shown by Figure 1 and Eq. (5) and (6), generation of [RO] is governed by the radical [R] and oxygen [O_2], in which [R] and [O_2] are, respectively, an increasing and decreasing function of time. Therefore, the combined effect leads to the optimal (or peak) of the temporal profile of [RO].

(iv) The steady-state radical produced by the enhancer [B] given by k_5[RO]= k_3 ([R][O_2]/[M]), is an increasing function of oxygen [O_2] and rate constant k_3, but a decreasing function of k_5, which is inverse proportional to the lifetime of [RO], i.e., high conversion requires a long lifetime (or smaller k_5).

We suggest that readers should read the measured data reported by Bonardi *et al* [19], which also explained the important features as predicted by our analytic formulas and our numerical results. For a more comprehensive modeling, readers may refer to Ref. [20]. This article explores the kinetics of a single-wavelength system. We also suggest readers to read our other articles which further explored 2-wavelength and 3-wavelength polymerizations [23], [24] for the applications in 3D bioprinting.

IV. CONCLUSION

We have demonstrated that efficacy of NIR photopolymerization could be enhanced by an enhancer [B] via dual function of (i) regeneration of the dye [C], and (ii) producing extra radical [RO]. The conversion is an increasing function of enhancer and oxygen concentration, and the coupling constant, b′= bI_0. However, they have significantly different steady state feature. High conversion also requires a long lifetime (or smaller k_5) of the free radical [RO]. The steady-state conversion increases from 10% without the enhancer (with enhancer concentration $[B]_0$ = 0) to (30%, 50%, 80%) for $[B]_0$=(0.5, 1.0, 2.0)%. Initiator concentration C(t) increases in the presence of enhancer ([B]). In contrast, a reversed trend is shown by Figure 5, in which a larger coupling (b′) leads to a stronger depletion of C(t). Generation of [RO] is governed by the radical [R] and oxygen [O_2] and the combined effect leads to the optimal (or peak) of the temporal profile of [RO].

CONFLICTS OF INTEREST

Jui-Teng Lin is the CEO of Photon Vision Corp., Taipei, Taiwan. The funders had no role in the design of the study; in the collection, analyses, or interpretation of data; in the writing of the manuscript, or in the decision to publish the results.

ACKNOWLEDGMENT

The authors are grateful to the National Center for High-performance Computing for computer time and facility.

REFERENCES

[1] G. Odian, *Principles of Polymerization*, 4th ed. New York, NY, USA: Wiley 2006.
[2] J.-P. Fouassier, "Fundamentals and applications," in *Photoinitiation, Photopolymerization, and Photocuring*. Munich, Germany: Hanser Gardner, 1995.
[3] Y. Yagci, S. Jockusch, and N. J. Turro, "Photoinitiated polymerization: Advances, challenges, and opportunities," *Macromolecules*, vol. 43, no. 15, pp. 6245–6260, Aug. 2010.
[4] J. Jakubiak, X. Allonas, J. P. Fouassier, A. Sionkowska, E. Andrzejewska, L. Å. Linden, and J. F. Rabek, "Camphorquinone–amines photoinitating systems for the initiation of free radical polymerization," *Polymer*, vol. 44, no. 18, pp. 5219–5226, Aug. 2003.
[5] Y. Bi and D. C. Neckers, "A visible light initiating system for free radical promoted cationic polymerization," *Macromolecules*, vol. 27, no. 14, pp. 3683–3693, Jul. 1994.
[6] W. D. Cook, "Photopolymerization kinetics of dimethacrylates using the camphorquinone/amine initiator system," *Polymer*, vol. 33, no. 3, pp. 600–609, Jan. 1992.

[7] J. Kabatc, J. Ortyl, and K. Kostrzewska, "New kinetic and mechanistic aspects of photosensitization of iodonium salts in photopolymerization of acrylates," *RSC Adv.*, vol. 7, no. 66, pp. 41619–41629, 2017.
[8] J. Kirschner, J. Paillard, M. Bouzrati-Zerelli, J.-M. Becht, J. E. Klee, S. Chelli, S. Lakhdar, and J. Lalevée, "Aryliodonium ylides as novel and efficient additives for radical chemistry: Example in camphorquinone (CQ)/Amine based photoinitiating systems," *Molecules*, vol. 24, no. 16, p. 2913, 2019.
[9] B. Strehmel, T. Brömme, C. Schmitz, K. Reiner, S. Ernst, and D. Keil, "NIR-dyes for photopolymers and laser drying in the graphic industry," in *Dyes and Chromophores in Polymer Science*. Hoboken, NJ, USA: Wiley, 2015, pp. 213–249.
[10] C. Schmitz, A. Halbhuber, D. Keil, and B. Strehmel, "NIR-sensitized photoinitiated radical polymerization and proton generation with cyanines and LED arrays," *Prog. Organic Coatings*, vol. 100, pp. 32–46, Nov. 2016.
[11] M. Bouzrati-Zerelli, M. Maier, C. P. Fik, C. Dietlin, F. Morlet-Savary, J. P. Fouassier, J. E. Klee, and J. Lalevée, "A low migration phosphine to overcome the oxygen inhibition in new high performance photoinitiating systems for photocurable dental type resins," *Polym. Int.*, vol. 66, no. 4, pp. 504–511, Apr. 2017.
[12] S. C. Ligon, B. Husár, H. Wutzel, R. Holman, and R. Liska, "Strategies to reduce oxygen inhibition in photoinduced polymerization," *Chem. Rev.*, vol. 114, no. 1, pp. 557–589, Jan. 2014.
[13] J.-T. Lin, H.-W. Liu, K.-T. Chen, and D.-C. Cheng, "Modeling the kinetics, curing depth, and efficacy of radical-mediated photopolymerization: The role of oxygen inhibition, viscosity, and dynamic light intensity," *Frontiers Chem.*, vol. 7, p. 760, Nov. 2019.
[14] K. T. Chen, D. C. Cheng, J. T. Lin, and H. W. Liu, "Thiol-ene photopolymerization in thick polymers: Kinetics and analytic formulas for the efficacy and crosslink depth," *Polymers*, vol. 11, no. 1640, pp. 3310–3390, 2019.
[15] M. Claudino, X. Zhang, and M. D. Alim, "Mechanistic kinetic modeling of thiol–Michael addition photopolymerizations via photocaged 'superbase' generators: An analytical approach," *Macromolecules*, vol. 49, no. 21, pp. 8061–8074, 2016.
[16] J.-T. Lin, "Kinetics of enhancement for corneal cross-linking: Proposed model for a two-initiator system," *Ophthalmol. Res., Int. J.*, vol. 10, pp. 1–6, Aug. 2019.
[17] K. T. Chen, J. T. Lin, and H. W. Liu, "Enhancing radical-mediated photopolymerization efficacy and crosslink depth: Kinetic modeling of a two-monomer system," *Res. Med. Eng. Sci.*, vol. 8, pp. 853–860, Aug. 2019.
[18] K. K. Childress, K. Kim, D. J. Glugla, C. B. Musgrave, C. N. Bowman, and J. W. Stansbury, "Independent control of singlet oxygen and radical generation via irradiation of a two-color photosensitive molecule," *Macromolecules*, vol. 52, no. 13, pp. 4968–4978, Jul. 2019.
[19] A. H. Bonardi, F. Dumur, T. M. Grant, G. Noirbent, D. Gigmes, B. H. Lessard, J.-P. Fouassier, and J. Lalevée, "High performance near-infrared (NIR) photoinitiating systems operating under low light intensity and in the presence of oxygen," *Macromolecules*, vol. 51, no. 4, pp. 1314–1324, Feb. 2018.
[20] J.-T. Lin, "Efficacy S-formula and Kinetics of non-oxygen-mediated (Type-I) and oxygen-mediated (Type-II) corneal cross-linking," *Ophthalmol. Res., Int. J.*, vol. 8, no. 1, pp. 1–11, 2018.
[21] J.-T. Lin and D.-C. Cheng, "Modeling the efficacy profiles of UV-light activated corneal collagen crosslinking," *PLoS ONE*, vol. 12, no. 4, 2017, Art. no. e0175002.
[22] J.-T. Lin, H.-W. Liu, K.-T. Chen, and D.-C. Cheng, "Modeling the optimal conditions for improved efficacy and crosslink depth of photo-initiated polymerization," *Polymers*, vol. 11, no. 2, p. 217, 2019.
[23] J.-T. Lin, D.-C. Cheng, K.-T. Chen, and H.-W. Liu, "Dual-wavelength (UV and blue) controlled photopolymerization confinement for 3D-printing: Modeling and analysis of measurements," *Polymers*, vol. 11, no. 11, p. 1819, 2019.
[24] J.-T. Lin, D.-C. Cheng, K.-T. Chen, Y.-C. Chiu, and H.-W. Liu, "3-wavelength (UV, blue, red) controlled photo-confinement for 3D-printing: Kinetics and modeling," *IEEE Access*, vol. 8, pp. 49353–49362, 2020.